Gutzwiller projected states for the math xmlns="http://www.w3.org/1998/Math/MathML">mrow>msub>mi>J/mi>mn>1/mn>/msub>mo>−/mo>msub>mi>J/mi>mn>2/mn>/msub>/mrow>/math> Heisenberg model on the Kagome lattice: Achievements and pitfalls

Yasir Iqbal, Francesco Ferrari, Aishwarya Chauhan, Alberto Parola, Didier Poilblanc, and Federico Becca

Gutzwiller-projected states for the J_1–J_2 Heisenberg model on the kagome lattice: achievements and pitfalls

Yasir Iqbal,[1, *] Francesco Ferrari,[2, †] Aishwarya Chauhan,[1, †] Alberto Parola,[3] Didier Poilblanc,[4] and Federico Becca[5]

[1]*Department of Physics and Quantum Centers in Diamond and Emerging Materials (QuCenDiEM) group, Indian Institute of Technology Madras, Chennai 600036, India*
[2]*Institute for Theoretical Physics, Goethe University Frankfurt, Max-von-Laue-Strae 1, D-60438 Frankfurt am Main, Germany*
[3]*Dipartimento di Scienza e Alta Tecnologia, Università dell'Insubria, Via Valleggio 11, I-22100 Como, Italy*
[4]*Laboratoire de Physique Théorique UMR-5152, CNRS and Université de Toulouse, F-31062, Toulouse, France*
[5]*Dipartimento di Fisica, Università di Trieste, Strada Costiera 11, I-34151 Trieste, Italy*
(Dated: September 20, 2021)

We assess the ground-state phase diagram of the J_1–J_2 Heisenberg model on the kagome lattice by employing Gutzwiller-projected fermionic wave functions. Within this framework, different states can be represented, defined by distinct unprojected fermionic Hamiltonians that include hopping and pairing terms, as well as a coupling to local Zeeman fields to generate magnetic order. For $J_2 = 0$, the so-called U(1) Dirac state, in which only hopping is present (such as to generate a π-flux in the hexagons), has been shown to accurately describe the exact ground state [Y. Iqbal, F. Becca, S. Sorella, and D. Poilblanc, Phys. Rev. B **87**, 060405 (2013); Y.-C. He, M. P. Zaletel, M. Oshikawa, and F. Pollmann, Phys. Rev. X **7**, 031020 (2017)]. Here, we show that its accuracy improves in presence of a small *antiferromagnetic* super-exchange J_2, leading to a finite region where the gapless spin liquid is stable; then, for $J_2/J_1 = 0.11(1)$, a first-order transition to a magnetic phase with pitch vector $\mathbf{q} = (0,0)$ is detected, by allowing magnetic order within the fermionic Hamiltonian. Instead, for small *ferromagnetic* values of $|J_2|/J_1$, the situation is more contradictory. While the U(1) Dirac state remains stable against several perturbations in the fermionic part (i.e., dimerization patterns or chiral terms), its accuracy clearly deteriorates on small systems, most notably on 36 sites where exact diagonalization is possible. Then, upon increasing the ratio $|J_2|/J_1$, a magnetically ordered state with $\sqrt{3} \times \sqrt{3}$ periodicity eventually overcomes the U(1) Dirac spin liquid. Within the ferromagnetic J_2 regime, evidence is shown in favor of a first-order transition at $J_2/J_1 = -0.065(5)$.

I. INTRODUCTION

The Heisenberg Hamiltonian

$$\hat{\mathcal{H}} = \sum_{i,j} J_{i,j}\hat{\mathbf{S}}_i \cdot \hat{\mathbf{S}}_j, \tag{1}$$

for spin-S operators, $\hat{\mathbf{S}}_i = (\hat{S}_i^x, \hat{S}_i^y, \hat{S}_i^z)$, arranged on a crystal lattice, represents one of the pillars of condensed-matter physics, capturing fundamental phenomena in quantum magnetism, such as symmetry breaking with Goldstone excitations, quantum phase transitions, topological order, and fractionalization emerging from exotic ground states [1, 2]. Particularly interesting are the cases with small spins (e.g., $S = 1/2$) on highly-frustrated low-dimensional lattices (e.g., featuring a triangular *motif*), for which there is increasing theoretical and experimental evidence that unconventional phases, which cannot be described by standard mean-field approaches, may settle down at sufficiently low temperatures [2, 3]. Solid theoretical evidence for the existence of spin-liquid phases has been worked out in models with spin anisotropic super-exchange couplings, most notably the compass Kitaev model on the honeycomb lattice,

which represents a unique example of a non-trivial spin model that can be exactly solved in two spatial dimensions. Here, both gapped and gapless phases are present as ground states, as well as an interesting chiral state in presence of a (small) external magnetic field [4]. By contrast, for Heisenberg models with SU(2) spin symmetry, the situation is more debated. A predominant example, which has been intensively investigated in the recent past, is given by the $S = 1/2$ Heisenberg model on the kagome lattice with nearest-neighbor antiferromagnetic coupling ($J_1 > 0$) only. The principal motivation comes from both experimental and theoretical reasons. As far as the former ones are concerned, it is remarkable that different families of materials may be synthesized, providing a clean realization of this spin model (e.g., perturbations coming from impurities, Dzyaloshinskii-Moriya or additional inter-plane interactions are relatively small compared to the nearest-neighbor super-exchange). This is the case for $ZnCu_3(OH)_6Cl_2$ [5–8], where no evidence for the insurgence of magnetic order is detected down to extremely small temperatures. From a theoretical point of view, the $S = 1/2$ Heisenberg model on the kagome lattice represents one of the major challenges in quantum magnetism, given its unconventional spectrum with an exceedingly large number of low-energy singlet excitations [9, 10].

A renewed effort to understand its physical properties followed from density-matrix renormalization group

(DMRG) calculations, which suggested the possibility that the ground state is a so-called $\mathbb{Z}_2$ spin liquid, with topological degeneracy and a finite spin gap [11, 12]. An alternative scenario suggested the stabilization of a gapless spin liquid, as proposed from a parton approach of the original spins [13, 14]. Here, Abrikosov fermions are introduced to define a mean-field Hamiltonian, with π-fluxes piercing the hexagonal plaquettes of the lattice. As a result, Dirac points are present in the free-fermion band structure. This state has been dubbed U(1) *Dirac state*, since the leading gauge fluctuations that emerge from the mean-field Hamiltonian have U(1) symmetry. When the Gutzwiller projector is considered, in order to construct a suitable variational wave function for the spin model, a remarkably accurate energy is obtained for the nearest-neighbor Heisenberg model [15]. In fact, further DMRG calculations with special boundary conditions [16, 17] supported the existence of Dirac cones in the spinon spectrum. Furthermore, tensor networks on the infinite lattice [18] also suggested a gapless spin liquid. This possibility immediately triggers the question of the stability of the gapless ground state against small perturbations.

Here, we consider the case where a next-nearest-neighbor super-exchange coupling (J_2) is included, with both ferromagnetic and antiferromagnetic character. In recent past, only few works have investigated the nature of the ground state of the J_1–J_2 Heisenberg model on the kagome lattice [18–22]. For $J_2/J_1 > 0$ an antiferromagnetic phase with $\mathbf{q} = (0,0)$ pitch vector is expected to exist for sufficiently large values of the next-nearest-neighbor interactions; instead, for $J_2/J_1 < 0$ another magnetically ordered phase with a $\sqrt{3} \times \sqrt{3}$ pattern is present. In addition, valence-bond crystals (VBCs), with possibly large unit cells (e.g., containing 12 or even 36 sites) may represent competitive states, as suggested in previous works [23–29].

Within the Abrikosov-fermion approach, different variational wave functions can be defined, by allowing different terms in the fermionic state, which can induce the opening of a spin gap (e.g., in a $\mathbb{Z}_2$ spin liquid), the breaking of translational symmetry (leading to a VBC), or the onset of magnetic order. The main outcome of the present paper is that the gapless spin liquid is stable in a finite region of the J_1–J_2 model. Indeed, for $J_2/J_1 > 0$, its accuracy to reproduce the exact ground-state improves with respect to the $J_2 = 0$ case, as indicated by a direct comparison with exact diagonalization on small clusters (the overlap between the gapless spin liquid and the exact ground state on 36 sites increases from 0.687 at $J_2 = 0$ to 0.875 at $J_2/J_1 = 0.05$). Then, by increasing the ratio J_2/J_1, the variational wave function develops magnetic order with $\mathbf{q} = (0,0)$, namely a finite Zeeman field can be stabilized (in the thermodynamic limit) within the fermionic Hamiltonian (on top of the hopping pattern of the π-flux state). The transition is located at $J_2/J_1 = 0.11(1)$ and is weakly first order, being characterized by a jump in the Zeeman field.
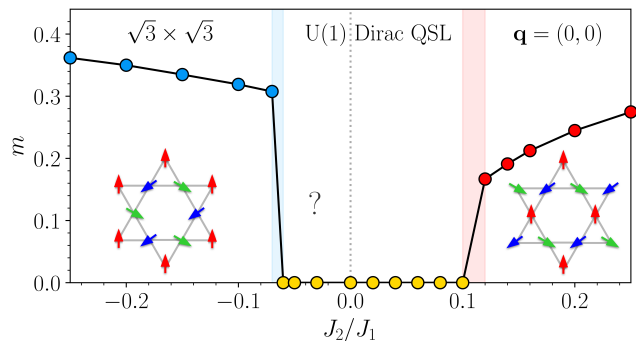

FIG. 1. The antiferromagnetic order parameter for the J_1–J_2 Heisenberg model on the kagome lattice. Different colors indicate the various ground-state phases: magnetic phases with $\mathbf{q} = (0,0)$ (red) or $\sqrt{3} \times \sqrt{3}$ periodicity (blue), and gapless spin liquid (yellow). The values are estimated in the thermodynamic limit (the error bars are smaller than the symbols), as shown below. The spin patterns for the two magnetically ordered phases are also shown. The U(1) Dirac state is expected to represent the paramagnetic region for $J_2 > 0$; instead, for $J_2 < 0$ the situation is more controversial.

For $J_2/J_1 < 0$, the situation is more delicate. For small values of $|J_2|/J_1$ the gapless spin-liquid wave function remains stable when allowing additional terms in the fermionic state. Upon increasing $|J_2|/J_1$, its variational energy is overcome by a different Gutzwiller-projected state, with $\sqrt{3} \times \sqrt{3}$ magnetic order and hopping terms with a different flux pattern (π flux on hexagons and up triangles, and zero flux on down triangles). The transition to a magnetically ordered phase is found at $J_2/J_1 = -0.065(5)$. In addition, VBC states with large unit cells (e.g., 36 sites) may also be stabilized and have competing energies close to the magnetic transition. The variational phase diagram, as obtained within our approach, is shown in Fig. 1. However, some care must be put on small negative values of J_2, where the U(1) Dirac spin liquid no longer represents an accurate wave function, as shown upon a comparison to the exact ground state on small clusters. This is due to the presence of level crossings (on 12 sites) or avoided crossings (on 36 sites) that happen in the low-energy singlet sector when varying J_2/J_1 close to $J_2 = 0$. Whether these crossings correspond to some phase transition in the thermodynamic limit is hard to resolve. Still, the situation remains more controversial on the $J_2 < 0$ side of the phase diagram, suggesting that an alternative approach may be needed when ferromagnetic super-exchange couplings are present.

The paper is organized as follows: in Section II, we describe the variational method that has been used; in Section III, we discuss our numerical results; finally, in Section IV, we draw our conclusions.

II. VARIATIONAL WAVE FUNCTIONS

The Abrikosov-fermion representation allows us to express the $S = 1/2$ spin operators as products of fermionic creation and annihilation operators [30–32]:

$$\hat{\mathbf{S}}_i = \frac{1}{2} \sum_{\alpha,\beta} \hat{c}^\dagger_{i,\alpha} \boldsymbol{\sigma}_{\alpha,\beta} \hat{c}_{i,\beta}, \qquad (2)$$

where $\boldsymbol{\sigma} = (\sigma_x, \sigma_y, \sigma_z)$ is a vector of Pauli matrices and $\hat{c}^\dagger_{i,\alpha}$ ($\hat{c}_{i,\alpha}$) creates (destroys) a fermion at site i with spin $\alpha = \uparrow, \downarrow$. This representation fulfills the spin commutation relations, but enlarges the Hilbert space of the system by including unphysical states with empty or doubly-occupied sites. The variational states employed in this work are defined by projecting Abrikosov-fermion wave functions into the physical spin space by using the Gutzwiller projector

$$\hat{\mathcal{P}}_G = \prod_i (\hat{n}_{i,\uparrow} - \hat{n}_{i,\downarrow})^2, \qquad (3)$$

where $\hat{n}_{i,\alpha} = \hat{c}^\dagger_{i,\alpha} \hat{c}_{i,\alpha}$. The fermionic state $|\Phi_0\rangle$ is obtained as the ground state of a noninteracting Hamiltonian, featuring hopping, pairing, and a fictitious Zeeman field. In particular, different symmetries of the pairing term can be considered, following the classifications of Ref. [33]. However, the variational minimization suggests that they are not stabilized for the values of J_2/J_1 considered in this work. Then, the best wave function is obtained from a noninteracting Hamiltonian that contains only hoppings and Zeeman fields:

$$\hat{\mathcal{H}}_0 = \sum_{(i,j),\alpha} \chi_{ij} \hat{c}^\dagger_{i,\alpha} \hat{c}_{j,\alpha} + h \sum_i \mathbf{M}_i \cdot \hat{\mathbf{S}}_i. \qquad (4)$$

In the following, we will include nearest- and next-nearest-neighbor hopping, $|\chi_1| = 1$ (to fix the energy scale) and χ_2 (as a variational parameter), respectively; an additional parameter is the amplitude of the magnetic field h, while the spatial periodicity is fixed by the unit vector $\mathbf{M}_i$, which lies in the XY plane, i.e., $\mathbf{M}_i = [\cos(\mathbf{q} \cdot \mathbf{R}_i + \phi_i), \sin(\mathbf{q} \cdot \mathbf{R}_i + \phi_i), 0]$ (where $\mathbf{q}$ is the pitch vector, $\mathbf{R}_i$ is the coordinate of the unit cell of site i, and ϕ_i is a sublattice-dependent angle). The same Hamiltonian may also give rise to VBC states, by setting $h = 0$ and allowing hoppings to break the space group symmetries, e.g., considering different values of $|\chi_1|$ and $|\chi_2|$ for different bonds within an enlarged unit cell [25, 26]. Additionally, a spin-spin Jastrow factor is included:

$$\hat{\mathcal{J}}_z = \exp\left(\frac{1}{2} \sum_{ij} u_{ij} \hat{S}^z_i \hat{S}^z_j \right), \qquad (5)$$

where u_{ij} defines a set of additional variational parameters, one for each distance $|\mathbf{R}_i - \mathbf{R}_j|$. Finally, the projection $\hat{\mathcal{P}}_z$ onto the subspace with $\sum_i \hat{S}^z_i = 0$ is also

performed. As a result, the variational wave function is written as

$$|\Psi_{\text{var}}\rangle = \hat{\mathcal{J}}_z \hat{\mathcal{P}}_z \hat{\mathcal{P}}_G |\Phi_0\rangle. \qquad (6)$$

It is worth mentioning that the existence of magnetic long-range order is directly related to the presence of a finite parameter h in the thermodynamic limit. Within magnetically ordered phases, the Jastrow factor of Eq. (5) plays an indispensable role by introducing transverse quantum spin fluctuations around the classical spin state [34]. In contrast to the previous study [20], performed with two different *Ansätze* for magnetic and non-magnetic states, the present choice, based upon the non-interacting Hamiltonian (4) allows us to have a unique framework for these phases, also including VBC.

As previously mentioned, the U(1) Dirac spin liquid represents a very accurate variational wave function for the nearest-neighbor model ($J_2 = 0$). This state is defined by a fermionic Hamiltonian $\hat{\mathcal{H}}_0$ with hopping terms χ_1 generating a π-flux through hexagonal plaquettes and 0-flux through triangles [33] (an additional χ_2 gives a small energy gain). For sufficiently large values of the next-neighbor super-exchange, the ground state acquires magnetic order, with two different pitch vectors depending on the sign of J_2, see Fig. 1. On the one hand, in the $\mathbf{q} = (0,0)$ ordered phase, the optimal noninteracting Hamiltonian $\hat{\mathcal{H}}_0$ contains a translationally invariant magnetic field (with sublattice angles ϕ_i such as to have a relative 120° orientation between neighboring spins in the unit cell) and the same hopping structure of the U(1) Dirac state. On the other hand, within the $\sqrt{3} \times \sqrt{3}$ ordered phase, a magnetic unit cell of 9 sites is required, with neighboring spins still having a relative 120° orientation (see Fig. 1). The optimal variational Ansatz is constructed from the Hamiltonian with a $\mathbf{q} = (4\pi/3a, 0)$ magnetic field (where a is the length of the Bravais lattice vectors) and the hopping terms of a different U(1) state, dubbed $[\pi, \pi]$, with π fluxes through hexagons and up triangles (and 0 flux through down triangles) [33].

Our variational calculations are mostly performed on $N = 3 \times L \times L$ clusters, with a few exceptions (including results of Lanczos diagonalization) in which the tilted $N = 9 \times L \times L$ clusters have been employed. All the finite-size clusters considered in this work fulfill the point group symmetries of the kagome lattice, and periodic boundary conditions for the Heisenberg Hamiltonian are imposed. On the contrary, the fermionic Hamiltonian (4) may have periodic or antiperiodic boundary conditions along the two vectors that define the cluster. Among these four possibilities, one of them gives rise to zero-energy modes in the fermionic spectrum of the U(1) Dirac state. The other three choices give the same variational energy after Gutzwiller projection, however, each one of them breaks rotational symmetries on finite clusters [35]. Within the variational calculations, one of these three possibilities has been considered. To evaluate the expectation values for a given variational state, we perform a quantum Monte Carlo sampling [36]. For the optimization of the

variational parameters we make use of the stochastic reconfiguration technique [37].

III. RESULTS

Let us now discuss our variational results. First of all, we investigate the case with antiferromagnetic next-nearest-neigbor super-exchange, i.e., $J_2/J_1 > 0$. Here, we consider a variational wave function that is generated from the uncorrelated Hamiltonian (4), including a fictitious Zeeman field with $\mathbf{q} = (0,0)$. In this regime, the best choice of the hoppings is such to obtain the U(1) Dirac state. In particular, both nearest- and next-nearest-neighbor hoppings are allowed [25], which together with the antiferromagnetic parameter h and all the independent u_{ij}'s of the spin-spin Jastrow factor (5) constitute the variational parameters. After optimizing on cluster sizes up to $L = 24$ (with 190 variational parameters, among which 188 for the Jastrow factor), we find that for $J_2/J_1 \geqslant 0.12$, the h parameter extrapolates to a finite value in the thermodynamic limit [see Fig. 2(a)], suggesting the existence of magnetic order. By contrast, for $J_2/J_1 \leqslant 0.10$, strong frustration is able to stabilize a quantum spin-liquid ground state; indeed, here the h parameter goes to zero as $1/L^2$ for $L \to \infty$, consistently with a power-law decay of the spin-spin correlations of the U(1) Dirac state [38] [see Fig. 2(a)]. We remark that, on each finite cluster, the Jastrow factor always leads to an improvement of the variational energy, although in the spin-liquid regime the effect is less pronounced.

Previous studies [18, 19, 21, 22, 39–42] [see Table I] investigated the onset of magnetic order for $J_2 > 0$. Apart from one-loop pseudo-fermion functional renormalization group calculations [19] (which are expected to be significantly altered at high-loop orders where convergence is reached), all other methods obtained values ranging between $J_2/J_1 \approx 0.05$ and ≈ 0.20. Our estimate of the transition point lies in this range, slightly smaller than DMRG calculations [21, 22] but larger than the tensor-network evaluation [18]. We mention that in a previous work of ours [20], we used a simplified variational wave function to describe the magnetic phase [including only the fictitious magnetic field h but not the fermionic hopping in Eq. (4)], leading to a substantial shift of the magnetic transition to larger values of J_2/J_1 (or, in other words, enlarging the stability region of the spin liquid by reducing the variational manifold of the magnetic states).

In order to have solid evidence for magnetic ordering, we compute the sublattice magnetization m, which is obtained from the expectation value of the spin-spin correlation at maximum distance (for two spins within the same sublattice):

$$m^2 = \lim_{|i-j| \to \infty} \langle \hat{\mathbf{S}}_i \cdot \hat{\mathbf{S}}_j \rangle \qquad (7)$$

for the variational state $|\Psi_{\text{var}}\rangle$. The magnetization displays a similar scaling as the h parameter, thus confirming the extent of the spin-liquid regime, see Fig. 2(b). The magnetization estimate in the thermodynamic limit is shown in Fig. 1. Here, we observe a relatively sharp jump in m upon traversing the phase boundary, suggesting that the transition is not continuous. Since, a continuous transition between the U(1) Dirac spin liquid and the $\mathbf{q} = (0,0)$ state is, in principle, allowed [43], we attempt to ascertain the order of the phase transition in our numerical simulations. For this purpose, we chart out the variational energy landscape as a function of the fictitious Zeeman field h: this is done by fixing the field h to a grid of different values and optimizing only the remaining variational parameters to get the lowest energy. In Fig. 3, we show this energy landscape for different system sizes and for two values of J_2/J_1, one on either side of the transition. At $J_2/J_1 = 0.10$ (i.e., inside the spin-liquid regime), there are two minima: the lowest-energy one, extrapolating to $h = 0$ in the thermodynamic limit, and another one at higher energy for finite field $h \approx 0.3$. A finite-size scaling of the energy difference between these minima shows that it remains finite in the thermodynamic limit. At $J_2/J_1 = 0.12$ (i.e., inside the magnetic regime), the two minima switch, the one at $h \approx 0.3$ corresponding now to the lowest energy. The energies for the two possible states (with small and large Zeeman fields) are shown in Fig. 4 as a function of J_2/J_1. Hence, our variational approach clearly indicates that, in the thermodynamic limit, the best-energy solution has a jump from $h = 0$ to a finite value for $J_2/J_1 = 0.11(1)$, indicative of a first-order transition.

Let us now discuss the accuracy of the variational wave function when compared to the exact ground state for small finite-size lattices, e.g., the 36 sites cluster (namely, $9 \times 2 \times 2$, still possessing all the symmetries of the infinite kagome lattice). Here, in order to make a neat comparison with the exact ground state, we construct a fully-symmetric U(1) Dirac state (taking nearest-neighbor hoppings only). In fact, even though in Ref. [35] it was claimed that this is not possible on 36 sites, we verified that a suitable linear combination of the three possible choices of boundary conditions that do not give zero-energy modes corresponds to a state, $|\Psi_{\text{sym}}\rangle$, which lies in the same symmetry subspace of the exact ground state, $|\Psi_{\text{ex}}\rangle$. First of all, we compute the overlap between $|\Psi_{\text{sym}}\rangle$ with the first few exact eigenstates in the same symmetry subspace, as a function of J_2/J_1. The results are shown in Fig. 5, where the case of a small cluster with 12 sites is also reported. Remarkably, the overlap with the exact ground state increases when going from $J_2 = 0$ up to $J_2/J_1 \approx 0.05$.

Further highly convincing evidence that the ground-state wave function is well approximated by the U(1) Dirac spin-liquid Ansatz comes from performing the Lanczos technique, which allows us to obtain the exact ground state on a small cluster by an iterative procedure [44]. Starting from an arbitrary quantum state $|\Psi_0\rangle$, after p iterations, an estimate of the ground state is given
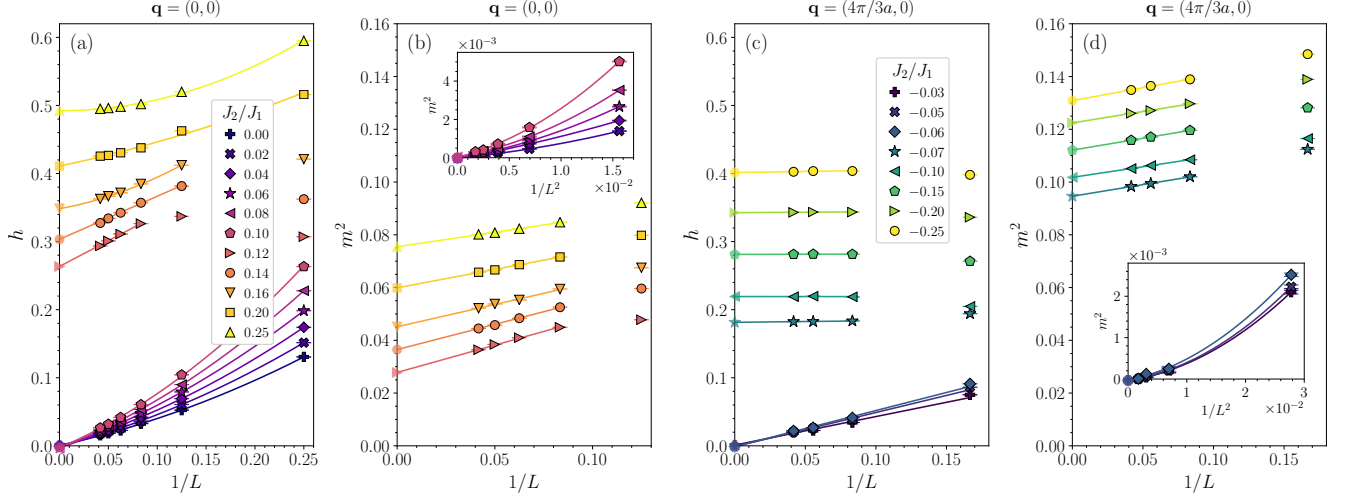
FIG. 2. Finite-size scalings of the fictitious Zeeman field h, see Eq. (4), and the square of the sublattice magnetization m^2 [panels (a) and (b) refer to the $\mathbf{q} = (0,0)$ order, panels (c) and (d) refer to the $\sqrt{3} \times \sqrt{3}$ order with $\mathbf{q} = (4\pi/3a, 0)$]. For $J_2 > 0$, we employed $3 \times L \times L$ clusters with $L = 4n$ ($n = 1, \ldots, 6$); for $J_2 < 0$ we used $L = 6n$ ($n = 1, \ldots, 4$). The hopping structure of the fermionic Hamiltonian (4) reproduces the $U(1)$ Dirac state for $J_2/J_1 \geqslant -0.06$, while it gives the $[\pi, \pi]$ state for $J_2/J_1 \leqslant -0.07$. The insets in (b) and (d) show the finite-size scaling of m^2 within the spin-liquid regime, as a function of $1/L^2$, which is consistent with a power-law decay of the spin-spin correlations of the $U(1)$ Dirac state [38].

	Phase I	Phase II	Method	J_2/J_1
			Variational Monte Carlo (present work)	0.11(1)
			Variational Monte Carlo [39]	0.08
			DMRG [21]	$0.15 - 0.20$
			DMRG [22]	0.20
J_2–Antiferromagnetic	Spin liquid	$\mathbf{q} = (0,0)$	Tensor networks [18]	0.045(10)
			Exact diagonalization [40]	0.16
			Exact diagonalization [41]	0.10
			Coupled-cluster method [42]	0.127
			One-loop PFFRG [19]	0.7
			Variational Monte Carlo (present work)	$-0.065(5)$
			DMRG [22]	-0.10
			Tensor networks [18]	-0.03
J_2–Ferromagnetic	Spin liquid	$\mathbf{q} = (4\pi/3a, 0)$	Exact diagonalization [40]	-0.06
			Exact diagonalization [41]	-0.10
			Coupled-cluster method [42]	-0.07
			One-loop PFFRG [19]	-0.4

TABLE I. The value of the transition between the spin-liquid and $\mathbf{q} = (0,0)$ (for $J_2 > 0$) and $\sqrt{3} \times \sqrt{3}$ (for $J_2 < 0$) magnetic orders obtained from our present calculations, compared to different methods for the J_1–J_2 Heisenberg model on the kagome lattice. Here, PFFRG stands for pseudo-fermion functional renormalization group.

by

$$|\Psi_p\rangle = \left(\sum_{k=0}^{p} \alpha_k \hat{\mathcal{H}}^k \right) |\Psi_0\rangle, \quad (8)$$

where the coefficients α_k are found by minimizing the energy

$$E_p = \langle \Psi_p | \hat{\mathcal{H}} | \Psi_p \rangle. \quad (9)$$

Here, we choose $|\Psi_0\rangle \equiv |\Psi_{\text{sym}}\rangle$ and compute the energy E_p as a function of the variance

$$\sigma_p^2 = \langle \Psi_p | \hat{\mathcal{H}}^2 | \Psi_p \rangle - \langle \Psi_p | \hat{\mathcal{H}} | \Psi_p \rangle^2, \quad (10)$$

which tends to zero when $p \to \infty$. The results are shown in Fig. 6 for different values of J_2/J_1. For both $J_2 = 0$ and 0.05, an approximately linear behavior $E_p \approx E_{\text{ex}} + \text{const} \times \sigma_p^2$ is observed, suggesting a smooth convergence of the initial wave function to the
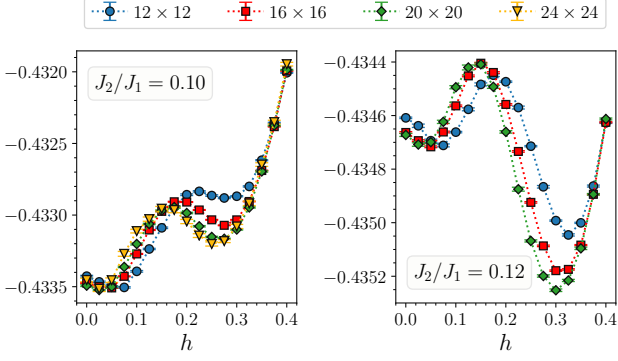
FIG. 3. Variational energy as a function of the fictitious Zeeman field h. The energy landscape has been computed for $J_2/J_1 = 0.10$ (left panel) and $J_2/J_1 = 0.12$ (right panel). Clusters with $3 \times L \times L$ sites have been used, with $L = 12$, 16, 20, and 24.
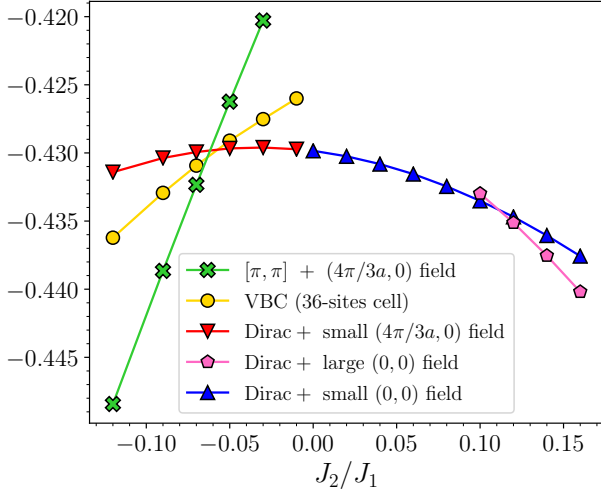

FIG. 4. Variational energies as a function of J_2/J_1 on the $9 \times 8 \times 8$ cluster. Different wave functions are considered, including a VBC state with 36 sites in the unit cell. When two local minima in the energy landscape are present (with small and large Zeeman fileds, as in Fig. 3), both variational energies are shown. We note that the energy landscape of the $[\pi, \pi]$ state with a $(4\pi/3a, 0)$ field has a single minimum as a function of h.

exact ground state. Indeed, an extrapolation of the total energy based on the first three steps of the Lanczos procedure ($p = 0, 1, 2$) gives $E/J_1 \approx -15.769$, compared to the exact value $E_{ex}/J_1 = -15.781$, for $J_2 = 0$. Similar results are also obtained for $J_2/J_1 = 0.05$, i.e., $E/J_1 \approx -15.826$ compared to $E_{ex}/J_1 = -15.835$. These results confirm the ones reported in Fig. 5, showing that the variational wave function has a large overlap with the exact ground state (for these values of J_2/J_1). Therefore, we are confident that the U(1) Dirac state faithfully represents the exact ground state of the Heisenberg model
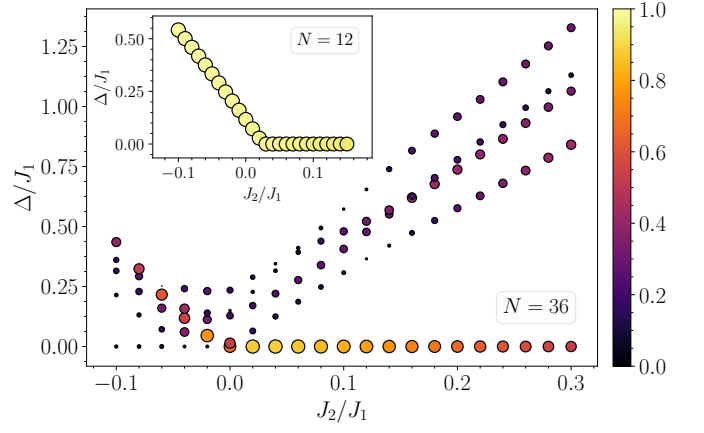

FIG. 5. Overlap between the symmetrized U(1) Dirac state $|\Psi_{sym}\rangle$ and few low-energy exact eigenstates on the 36-site cluster, obtained by Lanczos diagonalization. Both the area and the colors of the circles represent the value of the overlap. On the horizontal axis we report the value of J_2/J_1, while on the vertical axis we show the energy gap Δ of the exact eigenstates with respect to the ground state, in units of J_1. Notice that, the variational Ansatz $|\Psi_{sym}\rangle$ has a finite overlap only with the exact eigenstates belonging to the same symmetry sector. In the inset, analogous results on the 12-site cluster are reported.

on the kagome lattice, especially in presence of a small antiferromagnetic J_2/J_1.

Then, we move towards investigating the regime with ferromagnetic J_2, i.e., $J_2/J_1 < 0$. Here, we fix $\mathbf{q} = (4\pi/3a, 0)$ in the fermionic Hamiltonian (4). In Fig. 4, we compare the energies for different wave functions, corresponding to local minima in the variational energy landscape. While for $J_2/J_1 \geqslant -0.06$, the best Ansatz is given by the U(1) Dirac state with a small h parameter [eventually extrapolating to zero in the thermodynamic limit, see Fig. 2(c)], for $J_2/J_1 \leqslant -0.07$, the best state is magnetically ordered and obtained by employing a different flux pattern, i.e., the $[\pi, \pi]$ state defined in Ref. [33]. Therefore, a first-order transition is expected. A detailed size scaling of the magnetization is reported in Fig. 2(d), confirming the existence of a magnetic state for $J_2/J_1 \leqslant -0.07$. Our estimate of the phase boundary is in good agreement with those from other methods as shown in Table I. In previous works that used similar *Ansätze* for the ground-state wave function [25, 26], we proposed that the U(1) Dirac spin liquid should give way to a 36-site VBC for $J_2/J_1 \approx -0.045$; however, the present results, with magnetic ordering emerging for $J_2/J_1 \lesssim -0.06$, suggest that a phase with VBC order is highly unlikely, or may be stabilized only in a sliver of parameter space close to the $\sqrt{3} \times \sqrt{3}$ magnetic ordered region, see Fig. 4. Indeed, in this regime, the variational energies of the VBC candidates are similar to the ones of other competing states, i.e., the U(1) Dirac state and the magnetic one [28].

In spite of these variational results, we must emphasize that the accuracy of the spin-liquid wave function
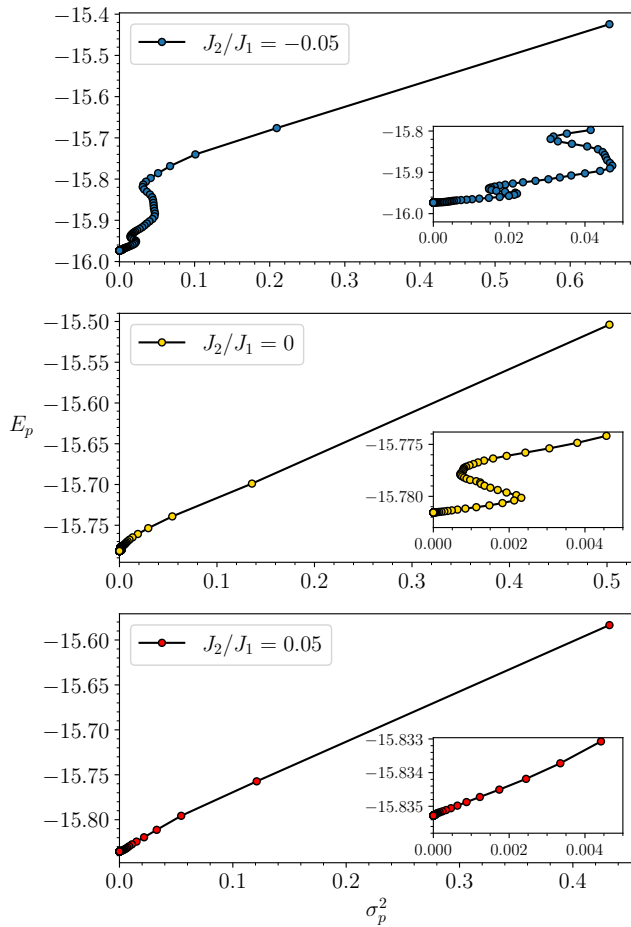
FIG. 6. Energy E_p [see Eq. (9)] versus variance σ_p^2 [see Eq. (10)] starting from the initial state given by the symmetrized U(1) Dirac Ansatz for three values of the ratio J_2/J_1. The energy (variance) is given in units of J_1 (J_1^2). Calculations are done for a cluster with 36 sites.

strongly deteriorates as soon as a small ferromagnetic J_2 is included. Indeed, the overlap of the symmetrized U(1) Dirac state with the exact ground state is very small, as shown in Fig. 5 for a 36-site cluster. Rather, the U(1) Dirac state has a significant overlap with an exact excited eigenstate. The Lanczos procedure also confirms that this variational state is not smoothly connected to the exact ground state, since the linear extrapolation converges to an energy that is well above the ground-state one, see Fig. 6. In fact, on the 36-site cluster there is an avoided crossing at $J_2/J_1 \approx 0$ (in the fully-symmetric subspace) [45]: the lowest-energy state for $J_2 > 0$ is well described by the U(1) Dirac spin liquid, while the one for $J_2 < 0$ is not. On 12 sites, a similar behavior is observed, with an actual level crossing for J_2 slightly larger than 0. These results put some doubts into the variational outcomes, for which the Dirac state remains stable up to $J_2/J_1 \approx -0.06$, with no other wave functions that we are able to construct, within the present Gutzwiller-projected states, having a lower energy. Indeed, we verified that both symmetric and lattice nematic $\mathbb{Z}_2$ [33] as well as chiral U(1) and $\mathbb{Z}_2$ [46] states cannot be stabilized (or are not energetically competing with the Dirac state). In addition, a few VBCs with 12-site unit cell (of the diamond type [11, 29]) have been assessed, with no gain in energy.

IV. CONCLUSIONS

In this work, we analyzed the $S = 1/2$ J_1–J_2 Heisenberg model by using a family of variational wave functions constructed from Abrikosov fermions, able to describe both spin liquid and magnetic phases *on the same footing.* This approach was previously shown to be successful for the case with nearest-neighbor interactions only [15]. Here, we provided evidence that, for antiferromagnetic values of the next-nearest-neighbor superexchange, the U(1) Dirac state remains stable up to $J_2/J_1 = 0.11(1)$; then, for larger values of J_2/J_1 a magnetically ordered state settles down, with $\mathbf{q} = (0,0)$ pitch vector, in agreement with other numerical methods [18, 21, 22, 39–42]. Note that, although a first order transition is found, a continuous transition between the Dirac state and the $\mathbf{q} = (0,0)$ magnetic phase is not forbidden [43]. Within the (gapless) spin-liquid regime, no energy gain is obtained by allowing pairing terms in the noninteracting fermionic Hamiltonian (4), in analogy to what has been emphasized for the case with $J_2 = 0$ [47, 48]. In addition, no VBC order has been detected by allowing nonuniform hopping amplitudes. The fact that the U(1) Dirac state faithfully represents the exact ground state of the J_1–J_2 model for $0 \lesssim J_2/J_1 \lesssim 0.10$ also follows from a direct comparison with exact calculations on small clusters. For example, on the 36-site cluster, a linear combination of Dirac states with three different boundary conditions can be constructed to have all the symmetries of the infinite lattice. This variational state (with no adjustable variational parameters) has quite a large overlap with the exact ground state, e.g., 0.875 for $J_2/J_1 = 0.05$.

By contrast, the ferromagnetic regime, i.e., $J_2/J_1 < 0$, is more problematic and asks for future investigations. Indeed, the U(1) Dirac state continues to give the lowest energy within Gutzwiller-projected fermionic *Ansätze* up to $J_2/J_1 = -0.065(5)$, where a magnetic state, with $\sqrt{3} \times \sqrt{3}$ periodicity, becomes the best variational wave function. No signal for opening of a spin gap has been detected for $-0.06 \lesssim J_2/J_1 \lesssim 0$, including the instability towards symmetric and lattice nematic $\mathbb{Z}_2$ spin liquids [33], U(1) and $\mathbb{Z}_2$ chiral spin liquids [46], or VBCs with different unit cells (most notably containing 12 or 36 sites) [25, 26]. Nonetheless, a comparison with exact calculations on small sizes shows that the U(1) Dirac state no longer accurately represents the ground state of the J_1–J_2 model. For example, on 36 sites for $J_2/J_1 = -0.05$, the overlap between the (symmetrized) spin-liquid state and the exact ground state is only 0.063. This fact

roots itself in the existence of an avoided crossing that changes the nature of the ground-state wave function. The resulting lowest-energy state does not seem to be described by any simple Gutzwiller-projected fermionic Ansatz. Whether this change in the low-energy sector is relevant for the true thermodynamic limit, or is only peculiar to the 36-site cluster is hard to ascertain. Certainly, the $J_2 = 0$ point is at the crossroads between different quantum phases (including the gapless spin liquid and magnetic phases, but possibly also VBC and chiral states, or even more exotic possibilities), and a crucial question to address in the future is the character of the several singlet states which populate the low-energy spectrum [49].

V. ACKNOWLEDGMENTS

[1] S. Sachdev, *Quantum Phase Transitions*, 2nd ed. (Cambridge University Press, 2011).

[2] L. Savary and L. Balents, Quantum spin liquids: a review, Rep. Prog. Phys. **80**, 016502 (2016).

[3] Y. Zhou, K. Kanoda, and T.-K. Ng, Quantum spin liquid states, Rev. Mod. Phys. **89**, 025003 (2017).

[4] A. Kitaev, Anyons in an exactly solved model and beyond, Ann. Phys. **321**, 2 (2006), january Special Issue.

[5] P. Mendels, F. Bert, M. de Vries, A. Olariu, A. Harrison, F. Duc, J. Trombe, J. Lord, A. Amato, and C. Baines, Quantum Magnetism in the Paratacamite Family: Towards an Ideal Kagomé Lattice, Phys. Rev. Lett. **98**, 077204 (2007).

[6] J. Helton, K. Matan, M. Shores, E. Nytko, B. Bartlett, Y. Yoshida, Y. Takano, A. Suslov, Y. Qiu, J.-H. Chung, D. Nocera, and Y. Lee, Spin Dynamics of the Spin-1/2 Kagome Lattice Antiferromagnet $ZnCu_3(OH)_6Cl_2$, Phys. Rev. Lett. **98**, 107204 (2007).

[7] M. de Vries, K. Kamenev, W. Kockelmann, J. Sanchez-Benitez, and A. Harrison, Magnetic Ground State of an Experimental $S = 1/2$ Kagome Antiferromagnet, Phys. Rev. Lett. **100**, 157205 (2008).

[8] M. Norman, Colloquium: Herbertsmithite and the search for the quantum spin liquid, Rev. Mod. Phys. **88**, 041002 (2016).

[9] P. Lecheminant, B. Bernu, C. Lhuillier, L. Pierre, and P. Sindzingre, Order versus disorder in the quantum Heisenberg antiferromagnet on the kagomé lattice using exact spectra analysis, Phys. Rev. B **56**, 2521 (1997).

[10] A. Läuchli, J. Sudan, and R. Moessner, $S = \frac{1}{2}$ kagome Heisenberg antiferromagnet revisited, Phys. Rev. B **100**, 155142 (2019).

[11] S. Yan, D. Huse, and S. White, Spin-Liquid Ground State of the $S = 1/2$ Kagome Heisenberg Antiferromagnet, Science **332**, 1173 (2011).

[12] S. Depenbrock, I. McCulloch, and U. Schollwöck, Nature of the Spin-Liquid Ground State of the $S = 1/2$ Heisenberg Model on the Kagome Lattice, Phys. Rev. Lett. **109**, 067201 (2012).

[13] M. Hastings, Dirac structure, RVB, and Goldstone modes in the kagomé antiferromagnet, Phys. Rev. B **63**, 014413 (2000).

[14] Y. Ran, M. Hermele, P. Lee, and X.-G. Wen, Projected-Wave-Function Study of the Spin-1/2 Heisenberg Model on the Kagomé Lattice, Phys. Rev. Lett. **98**, 117205 (2007).

[15] Y. Iqbal, F. Becca, S. Sorella, and D. Poilblanc, Gapless spin-liquid phase in the kagome spin-$\frac{1}{2}$ Heisenberg antiferromagnet, Phys. Rev. B **87**, 060405 (2013).

[16] Y.-C. He, M. Zaletel, M. Oshikawa, and F. Pollmann, Signatures of Dirac Cones in a DMRG Study of the Kagome Heisenberg Model, Phys. Rev. X **7**, 031020 (2017).

[17] W. Zhu, X. Chen, Y.-C. He, and W. Witczak-Krempa, Entanglement signatures of emergent Dirac fermions: Kagome spin liquid and quantum criticality, Sci. Adv. **4**, 11 (2018).

[18] H. Liao, Z. Xie, J. Chen, Z. Liu, H. Xie, R. Huang, B. Normand, and T. Xiang, Gapless Spin-Liquid Ground State in the $S = 1/2$ Kagome Antiferromagnet, Phys. Rev. Lett. **118**, 137202 (2017).

[19] R. Suttner, C. Platt, J. Reuther, and R. Thomale, Renormalization group analysis of competing quantum phases in the J_1-J_2 Heisenberg model on the kagome lattice, Phys. Rev. B **89**, 020408 (2014).

[20] Y. Iqbal, D. Poilblanc, and F. Becca, Spin-$\frac{1}{2}$ Heisenberg J_1-J_2 antiferromagnet on the kagome lattice, Phys. Rev. B **91**, 020402 (2015).

[21] S.-S. Gong, W. Zhu, L. Balents, and D. Sheng, Global phase diagram of competing ordered and quantum spin-liquid phases on the kagome lattice, Phys. Rev. B **91**, 075112 (2015).

[22] F. Kolley, S. Depenbrock, I. McCulloch, U. Schollwöck, and V. Alba, Phase diagram of the $J_1 - J_2$ Heisenberg model on the kagome lattice, Phys. Rev. B **91**, 104418 (2015).

[23] R. Singh and D. Huse, Ground state of the spin-1/2 kagome-lattice Heisenberg antiferromagnet, Phys. Rev. B **76**, 180407 (2007).

[24] G. Evenbly and G. Vidal, Frustrated Antiferromagnets with Entanglement Renormalization: Ground State of the Spin-$\frac{1}{2}$ Heisenberg Model on a Kagome Lattice, Phys. Rev. Lett. **104**, 187203 (2010).

[25] Y. Iqbal, F. Becca, and D. Poilblanc, Valence-bond crystal in the extended kagome spin-$\frac{1}{2}$ quantum Heisenberg antiferromagnet: A variational Monte Carlo approach, Phys. Rev. B **83**, 100404 (2011).

[26] Y. Iqbal, F. Becca, and D. Poilblanc, Valence-bond crystals in the kagome spin-1/2 Heisenberg antiferromagnet: a symmetry classification and projected wave function study, New J. Phys. **14**, 115031 (2012).

[27] Y. Huh, M. Punk, and S. Sachdev, Vison states and confinement transitions of $\mathbb{Z}_2$ spin liquids on the kagome lattice, Phys. Rev. B **84**, 094419 (2011).

[28] H. Changlani, S. Pujari, C.-M. Chung, and B. Clark, Resonating quantum three-coloring wave functions for the kagome quantum antiferromagnet, Phys. Rev. B **99**, 104433 (2019).

[29] A. Wietek and A. Läuchli, Valence bond solid and possible deconfined quantum criticality in an extended kagome lattice Heisenberg antiferromagnet, Phys. Rev. B **102**, 020411 (2020).

[30] G. Baskaran and P. Anderson, Gauge theory of high-temperature superconductors and strongly correlated Fermi systems, Phys. Rev. B **37**, 580 (1988).

[31] I. Affleck and J. Marston, Large-n limit of the Heisenberg-Hubbard model: Implications for high-T_c superconductors, Phys. Rev. B **37**, 3774 (1988).

[32] I. Affleck, Z. Zou, T. Hsu, and P. Anderson, SU(2) gauge symmetry of the large-U limit of the Hubbard model, Phys. Rev. B **38**, 745 (1988).

[33] Y.-M. Lu, Y. Ran, and P. Lee, $\mathbb{Z}_2$ spin liquids in the $S = \frac{1}{2}$ Heisenberg model on the kagome lattice: A projective symmetry-group study of Schwinger fermion mean-field states, Phys. Rev. B **83**, 224413 (2011).

[34] E. Manousakis, The spin-1/2 Heisenberg antiferromagnet on a square lattice and its application to the cuprous oxides, Rev. Mod. Phys. **63**, 1 (1991).

[35] M. Hermele, Y. Ran, P. Lee, and X.-G. Wen, Properties of an algebraic spin liquid on the kagome lattice, Phys. Rev. B **77**, 224413 (2008).

[36] F. Becca and S. Sorella, *Quantum Monte Carlo Approaches for Correlated Systems* (Cambridge University Press, 2017).

[37] S. Sorella, Wave function optimization in the variational Monte Carlo method, Phys. Rev. B **71**, 241103 (2005).

[38] F. Ferrari, A. Parola, and F. Becca, Gapless spin liquids in disguise, Phys. Rev. B **103**, 195140 (2021).

[39] T. Tay and O. Motrunich, Variational study of $J_1 - J_2$ Heisenberg model on kagome lattice using projected Schwinger-boson wave functions, Phys. Rev. B **84**, 020404 (2011).

[40] H. Changlani, D. Kochkov, K. Kumar, B. Clark, and E. Fradkin, Macroscopically Degenerate Exactly Solvable Point in the Spin-1/2 Kagome Quantum Antiferromagnet, Phys. Rev. Lett. **120**, 117202 (2018).

[41] P. Prelovsek, K. Morita, T. Tohyama, and J. Herbrych, Vanishing Wilson ratio as the hallmark of quantum spin-liquid models, Phys. Rev. Research **2**, 023024 (2020).

[42] J. Richter and O. Götze, unpublished.

[43] X.-Y. Song, C. Wang, A. Vishwanath, and Y.-C. He, Unifying description of competing orders in two-dimensional quantum magnets, Nat. Commun. **10**, 4254 (2019).

[44] N. Laflorencie and D. Poilblanc, Simulations of pure and doped low-dimensional spin-1/2 gapped systems, Lecture Notes in Physics , 227 (2004).

[45] T. Li, A continuous family of fully frustrated Heisenberg models on the Kagome lattice, EPL **133**, 47001 (2021).

[46] S. Bieri, C. Lhuillier, and L. Messio, Projective symmetry group classification of chiral spin liquids, Phys. Rev. B **93**, 094437 (2016).

[47] Y. Iqbal, F. Becca, and D. Poilblanc, Projected wave function study of $\mathbb{Z}_2$ spin liquids on the kagome lattice for the spin-$\frac{1}{2}$ quantum Heisenberg antiferromagnet, Phys. Rev. B **84**, 020407 (2011).

[48] Y. Iqbal, D. Poilblanc, R. Thomale, and F. Becca, Persistence of the gapless spin liquid in the breathing kagome heisenberg antiferromagnet, Phys. Rev. B **97**, 115127 (2018).

[49] Y. Yao, C. Umrigar, and V. Elser, Chemistry of the spin-$\frac{1}{2}$ kagome Heisenberg antiferromagnet, Phys. Rev. B **102**, 014413 (2020).